Structural and Morphological Attributes of Zn/Mg Doped β-tricalcium Phosphate for orthopedic applications

by Ali Taha Saleh

Submission date: 22-Jan-2021 09:46AM (UTC+0200)
Submission ID: 1492049072
File name: Ali-manuscript-1_2.docx (356.31K)
Word count: 2436
Character count: 14093

Structural and Morphological Attributes of Zn/Mg Doped β-tricalcium Phosphate for orthopedic applications

Ali Taha Saleh

Department of Chemistry, Collage of Science, University of Misan, Misan, Iraq.

Corresponding Author: Ali Taha Saleh: Email: ali_6222@yahoo.com.sg

Abstract

This paper reports the structural and morphological characteristics of some zinc (Zn) and magnesium (Mg) co-doped (at various contents) β-tricalcium phosphates (hereafter called ZMβTCPs) prepared using the microwave (MW) assisted wet precipitation method where the Ca deficient apatite [$Ca_{9-(x+y)}Mg_xZn_y(HPO_4)(PO_4)_5(OH)$] was calcined at 1000 ºC for 2 hr. As-prepared samples were characterized using the XRD, FTIR and FESEM measurements. The XRD patterns of the samples showed the steady decrease in the lattice parameters with the increase in $Mg^{2+}$and Zn^{2+} contents. The FESEM images of the samples disclosed the morphological changes due to the Mg^{2+}/Zn^{2+} co-doping. The inclusion of Mg^{2+} and Zn^{2+} into the βTCP was shown induce excellent bioactivities that were absent in the pristine TCP. As synthesized would be considered potential biodegradable material for orthopedic applications.

Keywords: ZMβTCP, Structure, Morphology, Co-doping, Phase purity, Crystallinity

1. Introduction

The exceptional bioactivities, biocompatibilities and osteoconductive traits of the calcium phosphates (CPs) based materials make them promising for diverse biomedical applications. They are very effective for the bone tissues implants in the dental and orthopaedic reconstructive medicines [1-4]. Presently, the hydroxyapatites (HAs) and β-tricalcium phosphates (βTCPs) are extensively used for the bone tissues grafting due to their non-stimulating nature of the bone generation and resorption inhibition [5, 6]. Both TCPs and HAs based materials with various trace elements (Zn and Mg) doping have been shown to stimulate the outstanding bioactivities that are completely absent in their parent counterparts [7, 8].

In recent years, the inclusion of different dopants (Mg^{2+}, Sr^{2+}, and Zn^{2+}) into the structure of the CPs received focused attention due to their significant role in diverse

biological processes [9]. Zinc is one of the most vital trace elements responsible for sundry cellular processes in the human body functions such as the DNA replications, behavioral responses, reproductions and virilities, bone generations, bone growths and wound healings. In addition, the element Zn play a significant part in the genetic expressions, cellular growth regulations and cell differentiations [10]. Recent study revealed a clinical correlation among the osteoporosis and deficiency of Zn in the human body [11]. The main reason for the biocompatibility of Zn is due to its matching ionic radius (0.075 nm) with the bone tissue element. Meanwhile, the slow resorption of the βTCP ceramics by the bone tissues make them highly biocompatible [12]. The element Mg participates in diverse biological activities of humans such as the cellular proliferations and differentiations, cell–matrix interactions and usual functions of the organs [13]. The significance of the Mg concerning the human bone structures is well-known especially the prevention of the potential risks related to the osteoporosis [14]. On top, Mg is crucial for the calcification processes, bone fragilities and minerals metabolic activities [15].

In view of the significance of the indispensable elements Zn/Mg in the human body functioning, some Zn/Mg co-doped β-tricalcium phosphates (ZMβTCPs) were synthesized via the microwave (MW) assisted wet precipitation technique and characterized using different analytical tools. The structures and morphologies of the as-prepared samples were evaluated as a function of varying Zn/Mg contents to determine the feasibility of achieving improved bioactivities. The results were analyzed, interpreted and discussed.

2. Materials and characterization procedures

Analytical grade high purity chemical reagents (Qrec, New Zealand) of calcium nitrate [$Ca(NO_3)_2{\cdot}4H_2O$], diammonium hydrogen phosphate [$(NH_4)_2HPO_4$)], magnesium nitrate [$(Mg(NO_3)_2.6H_2O)$], zinc nitrate [$Zn(NO_3)_2$] and ammonium hydroxide [(NH_4OH)] were utilized to prepare the ZMβTCPs. The samples crystal structures and purity of the phases were examined using the X-ray diffractometer (Bruker D8 Advance XRD). The samples morphology was imaged via a field emission scanning electron microscope (FESEM, Zeiss-LEO 1530). The elemental compositional analyses of the samples were carried out using an energy dispersive X-Ray spectrometer (EDX, Swift ED 3000 from Oxford instrument operated at 20 kV). The chemical functional groups in the samples were detected using the Fourier transform infrared spectroscopy (FTIR, Nicolet iS50 spectrometer) following the classic KBr pellet technique. The FTIR spectra (in the transmission mode) were

recorded in the range of 400–4000 cm^{-1} with 32 scans at a resolution of 4 cm^{-1}. All the characterizations of the calcined samples (at 1000 °C) were performed at room temperature.

3. Sample preparation

The pristine βTCP and ZMβTCP were made via the MW assisted wet precipitation technique where the Ca/P and (Ca+Mg+Zn)/P molar ratio was kept at 1.5. First, the [$Ca(NO_3)_2 \cdot 4H_2O$)] was dissolved in 100 mL of double distilled water (DDW) followed by the addition of [$(NH_4)_2HPO_4$)] drops and the mixture was stirred continuously. The mixture pH was set at 7.4 via the addition of NH_4OH solution (8 M). Next, the resultant mixture was processed for 5 min in a MW oven (SHARP, model R-218LS operated at 800 W) before being filtrated and rinsed using DDW. Thereafter, the filtered specimen was dried for 17 h in an oven at 80 ºC followed by the calcination for 2 h at 1000 ºC to achieve the βTCP. Same procedure was followed to prepare the ZMβTCP using appropriate quantities of [$Mg(NO_3)_2.6H_2O$)], [$Zn(NO_3)_2$] and [$Ca(NO_3)_2.4H_2O$]. Table 1 enlists the chemical compositions (in mol) of the produced samples with various concentrations of Zn and Mg with their respective codes. The production of the βTCP and ZMβTCP can be described using the following chemical reaction pathways:

Pathway I:

$$9\text{-}(x+y)Ca(NO_3)_2 + xMg(NO_3)_2 + yZn(NO_3)_2 + 6(NH_4)_2HPO_4 + 6NH_4OH \longrightarrow (Ca_{9-(x+y)}Mg_xZn_y)(HPO_4)(PO_4)_5(OH) + 18NHNO_3 + 5H_2O$$

pathway II:

$$Ca_{9-(x+y)}Mg_xZn_y(HPO_4)(PO_4)_5(OH) \xrightarrow{1000\ ^{\circ}C/2\ h} 3\left(Ca_3\frac{x+y}{3}Mg\frac{y}{3}Zn\frac{x}{3}\right)(PO_4)_2 + H_2O$$

Table 1: Chemical compositions (in mol) of the obtained samples with their codes.

Sample Code	$Ca(NO_3)_2.4H_2O$	$(NH_4)_2HPO_4$	$Mg(NO_3)_2$	$Zn(NO_3)_2$	Mg+Zn
βTCP	9	6	0.0	0.0	0.0
ZMβTCP0.4	8.6	6	0.2	0.2	0.4
ZMβTCP0.6	8.4	6	0.3	0.3	0.6
ZMβTCP0.8	8.2	6	0.4	0.4	0.8
ZMβTCP1.0	7.0	6	0.5	0.5	1.0

4. Results and discussion

Figure 1 displays the XRD patterns of the produced samples, which consisted of several crystalline peaks at 25.82°, 27.77°, 29.64°, 31.02°, 32.4756°, and 34.38° corresponding to the growth along the (1 0 1 0), (2 1 4), (3 0 0), (0 2 1 0), (1 2 8), and (2 2 0) lattice planer orientations. The observed indexed peaks were matched with JCPDS card number 09-0169 for the crystalline βTCP. Table 2 shows the lattice parameters, cell volume and degree of crystallinity of the studied samples obtained from the XRD data analyses. The obtained lattice planer directions for the pristine βTCP verified the growth of the hexagonal crystals with the lattice constants of $a = b = 10.4592$ A° and $c = 37.3914$ A° as depicted in Table 2. The inclusion of Mg^{2+}/Zn^{2+} into the βTCP lattice structures diminished the intensity of the Bragg's peaks accompanied by a shift toward higher diffraction angles (values of 2θ) as indicated in Figure 1. The observed reduction in the samples degree of crystallinities (from 88 to 64) were due to the replacement of the Ca^{2+} with larger ionic radii (0.99 A°) by the Mg^{2+} (0.65 A°) and Zn^{2+} (0.74 A°) with smaller ionic radii. Furthermore, the XRD pattern did not reveal any other crystalline phases, confirming the samples purity [9]. The intense XRD peak was used to calculate the mean crystallite diameter following the Debye–Scherrer formula. The obtained mean size of the βTCP and ZMβTCP was 36 nm and 28 nm, respectively. The lattice values of *a* and *c* were gradually decreased with rise in Mg^{2+} and Zn^{2+} contents (Table 2). These shortening in the lattice constants were mainly due to the substitution of the Ca^{2+} by Mg^{2+}/Zn^{2+}, where disparity in their ionic radii played a significant role. The values of *a* and *c* were reduced from 10.4452-10.4101 A° and 37.2217-37.3598 A°, respectively with the addition of Mg^{2+}/Zn^{2+} into the βTCP structures. Meanwhile, cell volumes of the samples were reduced from 3529.7787-3514.2751 $A°^3$ with the increase in Mg^{2+}/Zn^{2+} doping levels into the βTCP structures.

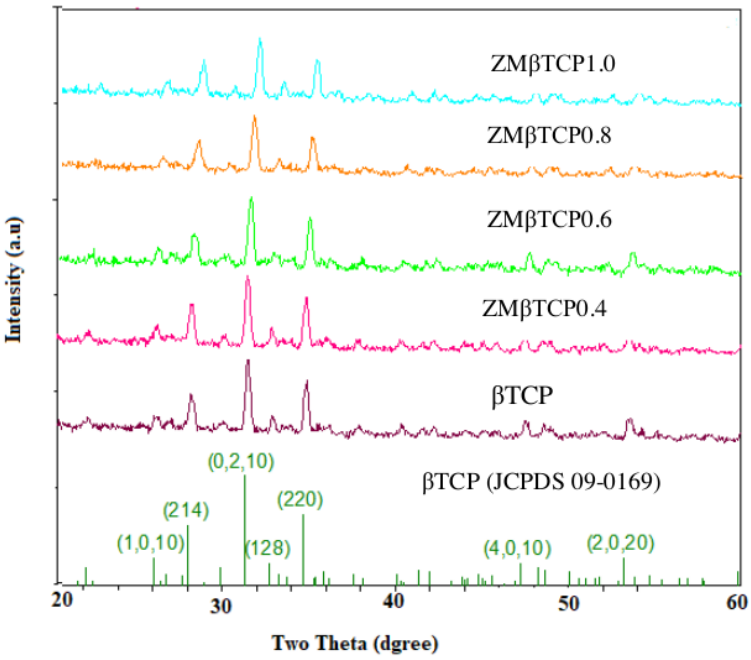

Figure 1: XRD patterns of the proposed samples.

Table 2: Lattice parameters, cell volume and degree of crystallinity of the studied samples.

Samples	Chemical formula	Lattice Parameters			Degree of crystallinity (%)
		a (A°)	*c* (A°)	V (A°^{3})	
βTCP	$Ca_9(PO_4)_6$	10.4592	37.3914	3532.6039	88
ZMβTCP0.4	$Ca_{8.6}MgZn_{0.4}(PO_4)_6$	10.4452	37.3598	3529.7787	81
ZMβTCP0.6	$Ca_{8.4}MgZn_{0.6}(PO_4)_6$	10.4212	37.3542	3524.0397	77
ZMβTCP0.8	$Ca_{8.2}MgZn_{0.8}(PO_4)_6$	10.4153	37.2541	3521.5517	69
ZMβTCP1.0	$Ca_{7.0}MgZn_{1.0}(PO_4)_6$	10.4101	37.2217	3514.2751	64

Figure 2 illustrates the FTIR spectra of all the prepared samples, which consisted of several characteristic vibration bands of the phosphate groups and water molecules. The pristine βTCP revealed broad vibration band at around 3440 cm^{-1} due to the OH^- from adsorbed water. The bands at approximately 1020 and 558 cm^{-1} were due to the vibration of the PO_4^{3-} units. The bands at around 618 and 548 cm^{-1} were related to the bending vibrations (υ_4) of the O–P–O linkages. The bands due the stretching vibrations (υ_3 and υ_1) of the P-O bond were occurred at approximately 955 cm^{-1}, 1033 and 1135 cm^{-1}. The bands appeared at around 1643 and 3448 cm^{-1} were due to the bond vibrations in the adsorbed

water. The characteristics bands at 962 cm^{-1}, 1122 cm^{-1} to 939 cm^{-1} and 1150 cm^{-1} corresponding to the phosphate vibrations were broadened and shifted as the doping contents of Mg^{2+}/Zn^{2+} were increased, implying the decrease in the samples crystallinity which is consistent with the XRD results (Figure 1). The nonexistence of the characteristic bands at 630 and 3570 cm^{-1} in the produced samples validated the complete absence of any HA as the secondary phase.

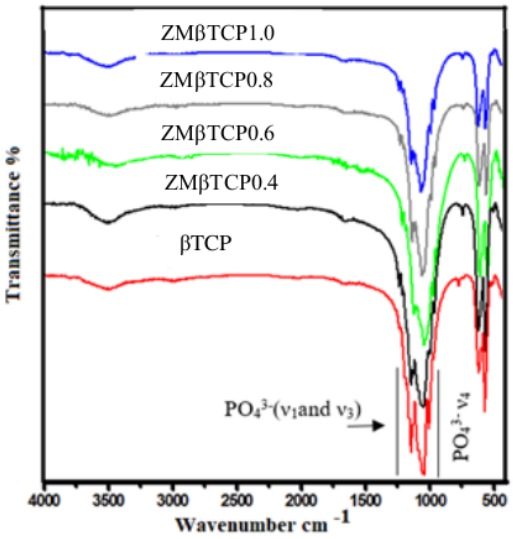

Figure 2: FTIR spectra of the studied samples.

Figure 3 depicts the FESEM images of all the produced samples. The microstructures of the βTCP were comprised of the dense (compact with nearly spherical crystallites without voids and cracks) aggregated particles with irregular morphology (Figure 3a). Moreover, the morphologies of the Mg^{2+}/Zn^{2+} co-doped βTCP specimens were appreciably altered into interconnected structures (less compact and ginger like pattern with many voids) with clustering tendency (Figure 3b-e).

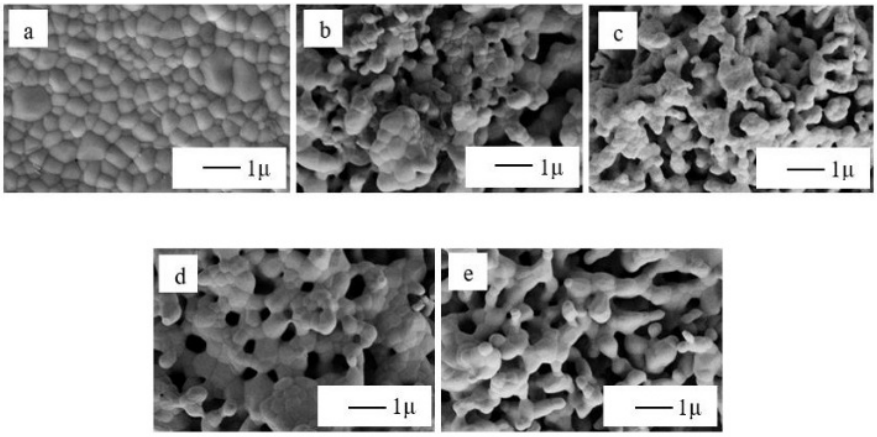

Figure 3: FESEM images of (a) βTCP, (b) ZMβTCP0.4, (c) ZMβTCP0.6, (d) ZMβTCP0.8 and (e) ZMβTCP1.0.

Table 3 compares the chemical composition of various products obtained from the EDX elemental analyses with the theoretical estimates. The close agreement between the theoretical and experimental values of the trace elemental ratios clearly confirmed the successful incorporation of the Mg^{2+}/Zn^{2+} into the βTCP crystals structure. In short, the inner-consistency among the XRD, FTIR and EDX results authenticated the effective replacement of Ca^{2+} by the Mg^{2+}/Zn^{2+} dopants in the βTCP lattice sites.

Table 3: Chemical composition of various products obtained from the EDX analyses when compared with the theoretical estimates.

Samples	**Theoretical ratios Mg/Zn/Ca+Mg/Zn = X_{MgZn}**	**Measured ratios Mg/Zn/Ca+Mg/Zn = X_{MgZn}**
βTCP	0.000	0.000
ZMβTCP0.4	0.040	0.038
ZMβTCP0.6	0.060	0.059
ZMβTCP0.8	0.080	0.078
ZMβTCP1.0	0.100	0.099

5. Conclusions

Following the standard MW assisted wet precipitation method, some Mg^{2+}/Zn^{2+} co-activated βTCP were produced. The Mg^{2+}/Zn^{2+} concentrations dependent structures and

morphologies of the dry and calcined (1000 ºC) powdered specimens were determined via thorough characterizations. The XRD analyses of the pristine and co-doped βTCP verified their hexagonal structure with phase purity where the lattice constants, cell volume, crystallinity and crystallite size were found to decrease with the increase in the Mg^{2+}/Zn^{2+} concentrations. The FTIR spectral vibration bands revealed the existence of various characteristics functional groups related to βTCP and ZMβTCP. The EDX analyses of the samples confirmed the appropriate elemental traces and thereby the successful incorporation of the Mg^{2+}/Zn^{2+} dopants into the βTCP lattice. The FESEM surface morphologies of the sample manifested the significant structural changes due to the substitution of Mg^{2+}/Zn^{2+} dopants, where more compact, void free, and dense agglomerated irregular structure were gradually transformed to less compact and interconnected cluster-like structures with many voids. The results for the structures and morphologies were in good agreement. All these observations were ascribed to the replacement of the Ca^{2+} with larger ionic radii by the Mg^{2+}/Zn^{2+} having smaller ionic radii. It is established that by selectively adjusting the Mg^{2+}/Zn^{2+} contents, the overall traits of the ZMβTCP can be tailored, suggesting their suitability towards diverse biomedical applications.

References

[1] D. Guo, K. Xu, X. Zhao, Y. Han, (2005) Development of a strontium-containing hydroxyapatite bone cement, *Biomaterials* 26(19) 4073-4083.

[2] B. Han, P.-W. Ma, L.-L. Zhang, Y.-J. Yin, K.-D. Yao, F.-J. Zhang, Y.-D. Zhang, X.-L. Li, W. Nie, (2009) β-TCP/MCPM-based premixed calcium phosphate cements, *Acta Biomaterialia* 5(8) 3165-3177.

[3] S. Wang, R. Liu, J. Yao, Y. Wang, H. Li, R. Dao, J. Guan, G. Tang, (2013) Fabrication of mesoporous magnesium substituted β-tricalcium phosphate nanospheres by self-transformation and assembly involving EDTA ions, *Microporous and Mesoporous Materials* 179 172-181.

[4] C. Prakash, S. Singh, B.S. Pabla, S.S. Sidhu, M.S. Uddin, (2019)Bio-inspired low elastic biodegradable Mg-Zn-Mn-Si-HA alloy fabricated by spark plasma sintering, *Materials and Manufacturing Processes* 34(4) 357-368.

[5] X. Yin, L. Calderin, M.J. Stott, M. Sayer, (2002)Density functional study of structural, electronic and vibrational properties of Mg- and Zn-doped tricalcium phosphate biomaterials, *Biomaterials* 23(20) 4155-4163.

[6] O. Kaygili, S. Keser, N. Bulut, T. Ates, (2018) Characterization of Mg-containing hydroxyapatites synthesized by combustion method, *Physica B: Condensed Matter* 537 63-67.

[7] H. Kawamura, A. Ito, S. Miyakawa, P. Layrolle, K. Ojima, N. Ichinose, T. Tateishi, (2000) Stimulatory effect of zinc-releasing calcium phosphate implant on bone formation in rabbit femora, J*ournal of Biomedical Materials Research* 50(2) 184-190.

[8] P. Shahmohammadi, B.A. Khazaei, (2021) Characterization of Zn/Mg-enriched calcium phosphate coating produced by the two-step pulsed electrodeposition method on titanium substrate, *Surfaces and Interfaces* 22 100819.

[9] A.T. Saleh, L.S. Ling, R. Hussain, (2016) Injectable magnesium-doped brushite cement for controlled drug release application, *Journal of Materials Science* 51(16) 7427-7439.

[10] A. Cuneyt Tas, S.B. Bhaduri, S. Jalota, (2007) Preparation of Zn-doped β-tricalcium phosphate (β-Ca3(PO4)2) bioceramics, *Materials Science and Engineering: C* 27(3) 394-401.

[11] P. Relea, M. Revilla, E. Ripoll, I. Arribas, L.F. Villa, H. Rico, Zinc, (1995)Biochemical Markers of Nutrition, and Type I Osteoporosis, *Age and Ageing* 24(4) 303-307.

[12] I.V. Fadeeva, M.R. Gafurov, I.A. Kiiaeva, S.B. Orlinskii, L.M. Kuznetsova, Y.Y. Filippov, A.S. Fomin, G.A. Davydova, I.I. Selezneva, S.M. Barinov, (2017)Tricalcium Phosphate Ceramics Doped with Silver, Copper, Zinc, and Iron (III) Ions in Concentrations of Less Than 0.5 wt.% for Bone Tissue Regeneration, *BioNanoScience* 7(2) 434-438.

[13] M.P. Hofmann, A.R. Mohammed, Y. Perrie, U. Gbureck, J.E. Barralet, (2009) High-strength resorbable brushite bone cement with controlled drug-releasing capabilities, *Acta Biomaterialia* 5(1) 43-49.

[14] M. Frasnelli, A. Pedranz, M. Biesuz, S. Dirè, V.M. Sglavo, (2019) Flash sintering of Mg-doped tricalcium phosphate (TCP) nanopowders, *Journal of the European Ceramic Society* 39(13) 3883-3892.

[15] S. Kannan, F. Goetz-Neunhoeffer, J. Neubauer, S. Pina, P.M.C. Torres, J.M.F. Ferreira, (2010) Synthesis and structural characterization of strontium- and magnesium-co-substituted β-tricalcium phosphate, *Acta Biomaterialia* 6(2) 571-576.

Structural and Morphological Attributes of Zn/Mg Doped β-tricalcium Phosphate for orthopedic applications

ORIGINALITY REPORT

18%	13%	14%	5%
SIMILARITY INDEX	INTERNET SOURCES	PUBLICATIONS	STUDENT PAPERS

PRIMARY SOURCES

1	link.springer.com Internet Source	5%
2	Submitted to Wright State University Student Paper	2%
3	Ammar Z. Alshemary, Yi-Fan Goh, Imran Shakir, Rafaqat Hussain. "Synthesis, characterization and optical properties of chromium doped β-Tricalcium phosphate", Ceramics International, 2015 Publication	1%
4	etd.uwaterloo.ca Internet Source	1%
5	www.karger.com Internet Source	1%
6	Bengi Yilmaz, Ammar Z. Alshemary, Zafer Evis. "Co-doped hydroxyapatites as potential materials for biomedical applications", Microchemical Journal, 2018 Publication	1%

7	iopscience.iop.org Internet Source	1%
8	www.mdpi.com Internet Source	1%
9	Weichang Xue. "Synthesis and characterization of tricalcium phosphate with Zn and Mg based dopants", Journal of Materials Science Materials in Medicine, 07/2008 Publication	1%
10	www.tandfonline.com Internet Source	1%
11	Faruk Küçükaşik, Hande Kazak, Dilvin Güney, Ilaria Finore et al. "Molasses as fermentation substrate for levan production by Halomonas sp.", Applied Microbiology and Biotechnology, 2010 Publication	<1%
12	www.researchsquare.com Internet Source	<1%
13	Hui Zhu, Dagang Guo, Wenli Qi, Kewei Xu. "Development of Sr-incorporated biphasic calcium phosphate bone cement", Biomedical Materials, 2017 Publication	<1%
14	Kannan, S.. "Synthesis and structural	<1%

characterization of strontium- and magnesium-co-substituted sz-tricalcium phosphate", Acta Biomaterialia, 201002
Publication

---

15 Ravi, Narmadha Devi, Rajkamal Balu, and T.S. Sampath Kumar. "Strontium-Substituted Calcium Deficient Hydroxyapatite Nanoparticles: Synthesis, Characterization, and Antibacterial Properties", Journal of the American Ceramic Society, 2012. <1%
Publication

---

16 pubs.rsc.org <1%
Internet Source

---

17 Araujo, J.C.. "Maximum substitution of magnesium for calcium sites in Mg-@b-TCP structure determined by X-ray powder diffraction with the Rietveld refinement", Materials Chemistry and Physics, 20091215 <1%
Publication

---

18 www.webqc.org <1%
Internet Source

---

19 Ali Motameni, Ali Deniz Dalgic, Ammar Z. Alshemary, Dilek Keskin, Zafer Evis. "Structural and Biological Analysis of Mesoporous Lanthanum Doped βTCP For Potential Use as Bone Graft Material", Materials Today Communications, 2020 <1%

Publication

20	Ali Taha Saleh, Lee Siew Ling, Rafaqat Hussain. "Injectable magnesium-doped brushite cement for controlled drug release application", Journal of Materials Science, 2016 Publication	<1%
21	www.hindawi.com Internet Source	<1%
22	Sanjeevi Kannan. "Synthesis and Structure Refinement of Zinc-Doped β-Tricalcium Phosphate Powders", Journal of the American Ceramic Society, 07/2009 Publication	<1%
23	Muthusamy Prabhu, Kandiah Kavitha, Palanisamy Manivasakan, Venkatachalam Rajendran, Palanisami Kulandaivelu. "Synthesis, characterization and biological response of magnesium-substituted nanobioactive glass particles for biomedical applications", Ceramics International, 2013 Publication	<1%

Exclude quotes	On	Exclude matches	< 1 words
Exclude bibliography	On		